NAVAL POSTGRADUATE SCHOOL
Monterey, California

THESIS

AN APPROACH FOR IMPRESSION CREEP OF LEAD FREE MICROELECTRONIC SOLDERS

by

Onofrio A. Anastasio

June 2002

Thesis Advisor: Indranath Dutta

Approved for public release; distribution is unlimited

THIS PAGE INTENTIONALLY LEFT BLANK

REPORT DOCUMENTATION PAGE

Form Approved OMB No. 0704-0188

1. AGENCY USE ONLY *(Leave blank)*	2. REPORT DATE	3. REPORT TYPE AND DATES COVERED
	June 2002	Master's Thesis

4. TITLE AND SUBTITLE
An Approach for Impression Creep of Lead-Free Microelectronic Solders

5. FUNDING NUMBERS

6. AUTHOR (S) Anastasio, Onofrio A.

7. PERFORMING ORGANIZATION
Naval Postgraduate School
Monterey, CA 93943-5000

8. PERFORMING ORGANIZATION REPORT NUMBER

9. SPONSORING / MONITORING AGENCY NAME(S) AND ADDRESS(ES)

10. SPONSORING/MONITORING AGENCY REPORT NUMBER

11. SUPPLEMENTARY NOTES The views expressed in this thesis are those of the author and do not reflect the official policy or position of the U.S. Department of Defense or the U.S. Government.

12a. DISTRIBUTION / AVAILABILITY STATEMENT
Approved for public release; distribution is unlimited

12b. DISTRIBUTION CODE

13. ABSTRACT ***(maximum 200 words)***

Currently, the microelectronics industry is transitioning from lead-containing to lead-free solders in response to legislation in the EU and Japan. Before an alternative alloy can be designated as a replacement for current Pb-Sn extensive testing must be accomplished. One major characteristic of the alloy that must be considered is creep. Traditionally, creep testing requires numerous samples and a long time, which thwarts the generation of comprehensive creep databases for difficult to prepare samples such as microelectronic solder joints. However, a relatively new technique, impression creep enables us to rapidly generate creep data. This test uses a cylindrical punch with a flat end to make an impression on the surface of a specimen under constant load. The steady state velocity of the indenter is found to have the same stress and temperature dependence as the conventional unidirectional creep test using bulk specimens.

This thesis examines impression creep tests of eutectic Sn-Ag. A testing program and apparatus was developed and constructed based on a servo hydraulic test frame. The apparatus is capable of a load resolution of 0.01N with a stability of ±0.1N, and a displacement resolution of 0.05μm with a stability of ±0.1μm. Samples of eutectic Sn-Ag solder were reflowed to develop the microstructure used in microelectronic packaging. Creep tests were conducted at various stresses and temperatures and showed that coarse microstructures creep more rapidly than fine microstructures in the tested regime.

14. SUBJECT TERMS	15. NUMBER OF PAGES
Impression creep, Lead-free solders	50
	16. PRICE CODE

17. SECURITY CLASSIFICATION OF REPORT	18. SECURITY CLASSIFICATION OF THIS PAGE	19. SECURITY CLASSIFICATION OF ABSTRACT	20. LIMITATION OF ABSTRACT
Unclassified	Unclassified	Unclassified	UL

NSN 7540-01-280-5500

Standard Form 298 (Rev. 2-89)
Prescribed by ANSI Std. 239-18

THIS PAGE INTENTIONALLY LEFT BLANK

Approved for public release; distribution is unlimited

AN APPROACH FOR IMPRESSION CREEP OF LEAD FREE MICROELECTRONIC SOLDERS

Onofrio A. Anastasio,
Lieutenant Commander, United States Navy
B.S. Engineering Technology, Texas Tech University,1991

Submitted in partial fulfillment of the
requirements for the degree of

MASTER OF SCIENCE IN MECHANICAL ENGINEERING

from the

NAVAL POSTGRADUATE SCHOOL
June 2002

Author: 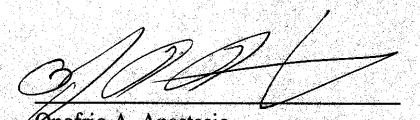
Onofrio A. Anastasio

Approved by: 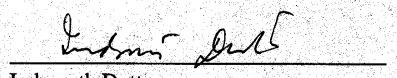
Indranath Dutta
Thesis Advisor

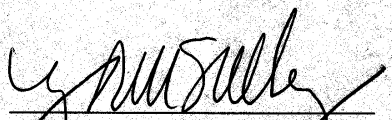
Terry R. McNelley
Chairman,
Department of Mechanical Engineering

iii

THIS PAGE INTENTIONALLY LEFT BLANK

ABSTRACT

Currently, the microelectronics industry is transitioning from lead-containing to lead-free solders in response to legislation in the EU and Japan. Before an alternative alloy can be designated as a replacement for current Pb-Sn extensive testing must be accomplished. One major characteristic of the alloy that must be considered is creep. Traditionally, creep testing requires numerous samples and a long time, which thwarts the generation of comprehensive creep databases for difficult to prepare samples such as microelectronic solder joints. However, a relatively new technique, impression creep enables us to rapidly generate creep data. This test uses a cylindrical punch with a flat end to make an impression on the surface of a specimen under constant load. The steady state velocity of the indenter is found to have the same stress and temperature dependence as the conventional unidirectional creep test using bulk specimens.

This thesis examines impression creep tests of eutectic Sn-Ag. A testing program and apparatus was developed and constructed based on a servo hydraulic test frame. The apparatus is capable of a load resolution of 0.01N with a stability of ±0.1N, and a displacement resolution of 0.05μm with a stability of ±0.1μm. Samples of eutectic Sn-Ag solder were reflowed to develop the microstructure used in microelectronic packaging. Creep tests were conducted at various stresses and temperatures and showed that coarse microstructures creep more rapidly than fine microstructures in the tested regime.

THIS PAGE INTENTIONALLY LEFT BLANK

TABLE OF CONTENTS

THIS PAGE INTENTIONALLY LEFT BLANK

LIST OF FIGURES

THIS PAGE INTENTIONALLY LEFT BLANK

LIST OF TABLES

THIS PAGE INTENTIONALLY LEFT BLANK

ACKNOWLEDGEMENTS

I would like to sincerely thank Professor Indranath Dutta for his guidance and support and making this project a worthwhile endeavor. I also want to give a special thanks to Keith Peterson, Sunglak Choi, and Chanman Park for all their help without which I could not have accomplished such a large project in a short period of time.

I would also like to thank my brother Michael, who made an extra effort during all the unforeseen events, so I could complete my research on time.

Lastly I would like to thank my wife who stood by me the whole way and never complained despite the late nights and long weekends at school.

THIS PAGE INTENTIONALLY LEFT BLANK

I. INTRODUCTION

Solder materials are utilized to provide electrical, thermal, and mechanical continuity between components in electronic applications. Sn-Pb solders have been extensively used as joining materials in electronic applications over the past several decades [1]. The widespread use of Sn-Pb solders is due to several advantages such as low cost, good manufacturability, and good wettability on common substrate such as Cu and Ni used in electronics. However, pending regulations regarding the use of solders containing Pb due to environmental and health concerns have put pressure on the electronics industry to find lead-free alternative for electronic applications. Increasing demands for greater packaging density and high performance are being realized with the advent of surface mount technology, resulting in the increase of the number of solder joints per package and reduction of joint dimensions. The international Technology Roadmap for Semiconductors (ITRS) [1] projects that the maximum size of high performance chips will increase from a 20mm square to a 25mm square, the power consumed will increase from 115 to 160W, and the peak temperature to which the chip may operate will increase from 155 to 175^{o}C. The ITRS also indicates that the maximum package pin count will (which correlates directly to the number of solder joints per chip and inversely with the solder joint size) will increase from 2007 to 3158.

In microelectronic packages using flip-chip (FC) and ball-grid array (BGA) interconnection schemes, solder balls of diameter 80 ~ 100 μm are employed. These tiny solder balls provide both electrical and mechanical connections between a Si chip and circuit board. There exists a large difference in the coefficient of thermal expansion (CTE) between the Si and the circuit board. This large difference in CTE induces thermal strain in the solder joint during service, which results in creep and/or fatigue deformation following thermal cycling. The thermal strains induced often result in a failure of solder joint and malfunction of the electronic package. Thus, the mechanical properties of the solder materials are crucial to the integrity of a solder joint, which in turn is vital to the reliability of the assembly.

Figure 1 shows the cross section of a FC package, where a Si-device is attached to an organic substrate, along with a solder joint located a distance x from the center of the chip. When the package is subjected to a temperature change ΔT, the solder joint undergoes plastic deformation in shear, where the thermal strain is given by:

$$g = \frac{(a_{substrate} - a_{chip})\Delta T x}{h} \quad (1)$$

where a is the CTE, and h is the height of the solder joint .

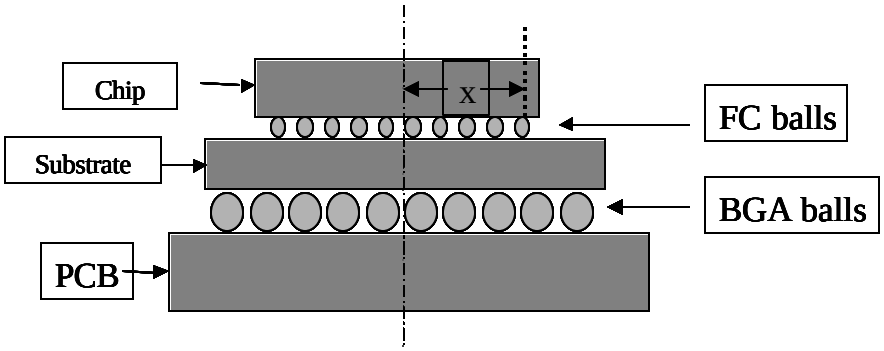

Figure 1. Basic cross section of an electronic package assembly.

When applying the projected increases in chip size, power and temperature to the strain equation it is easy to see that the solder joint will be operated under more severe service conditions.

Many Sn-based Pb-free solders have been proposed as alternatives to Sn-Pb solders. However, there is an insufficient amount of reliable creep data available and a significant disparity in the information available on these alloys [2]. It is therefore, important that a material property database of solder materials be established to develop a model for reliability prediction of solder joints that can be incorporated into electronic applications.

Since solder joint life is dictated largely by the creep strain range, which may be influenced appreciably by microstructural scale, it is important to develop new constitutive models for solder creep incorporating the effects of microstructural

coarsening, which can then be incorporated in finite element (FE) models for accurate prediction of joint reliability.

Tests simulating actual service conditions and conventional creep testing require many samples and are often time-consuming. It is also important to maintain the same microstructure when several samples are employed. Therefore a localized and relatively rapid creep testing method is attractive. One such method is a variation of indentation creep using a cylindrical indenter with a flat end. This type of test is called "impression creep."

The purpose of this thesis is to (1) develop an apparatus for impression creep testing of Pb-free solders, (2) demonstrate the functionality of the apparatus and (3) report preliminary creep data generated using this apparatus based on 96.5Sn-3.5Ag solders.

THIS PAGE INTENTIONALLY LEFT BLANK

II. BACKGROUND

A. LEAD-BEARING SOLDERS

In board level packaging, the material used is primarily Sn-Pb solder of either eutectic (63Sn-37Pb) or near-eutectic (60Sn-40Pb) composition. The melting point or range of Sn-Pb binary system allows soldering conditions that are compatible with most substrate materials and devices. A good understanding of Sn-Pb solders has enabled current board level technology to assemble and create small geometry solder joints, approaching 75 μm in size, in high volume and at competitive costs. However, there are legal, environmental and technological factors that are pressing for alternative Pb-free soldering materials and processing approaches. These factors include:

1. Emerging environmental regulations worldwide, most notably Europe and Japan have targeted the elimination of Pb usage in electronic assemblies due to the inherent toxicity of lead. Lead compounds have been cited by the Environmental Protection Agency (EPA) as one of the top 17 chemicals posing the greatest threat to human life and environment. When lead accumulates in the body over time, it inhibits normal processing and functions of the body. The concern about the use of lead in the electronics industry stems from occupational exposure, Pb waste derived from the manufacturing process and the disposal of electronic assemblies.
2. The continued trend towards packaging and interconnect miniaturization in Surface Mount Technology (SMT) is stretching the physical capability of Sn-Pb solder to provide sound and reliable solder joints [2].
3. There is also a need of employing different types of solders with different melting temperatures in step soldering of complex assemblies.
4. The need to improve device-performance by inducing less soft errors. Pb solders emit α-particles that can effect electronic package operations. Also recycled lead displays higher α-particle emissions that limit the recycle ability of Pb solders.

These concerns have made the search for Pb-free solders an important issue for microelectronic assemblies.

B. LEAD FREE SOLDERS

A large number of Pb free solders have been proposed. They include eutectic Sn-Ag, Sn-In, Sn-Zn, Sn-Bi, Sn-Sb, and Sn-Cu solders etc., and have Sn in common as a base metal [3,4]. Table 1 summarizes physical properties and cost of potential Pb-free solders [3,4,7]. The solders are binary, ternary, and some quaternary alloys.

Solders	M.P. (^oC)	CTE ($10^{-6}/^oC$)	Density (g/cm^3)	Cost ($/kg)
63Sn-37Pb	183	21	8.4	5.87
96.5Sn-3.5Ag	**221**	**22**	**7.36**	**13.73**
48Sn-52In	118	20	7.3	
42Sn-58Bi	138	15	8.7	7.79
91Sn-9Zn	199			7.99
99.3Sn-0.7Cu	227			8.62
95Sn-5Sb*	245	27		8.36

M.P. = Melting Point, CTE = Coefficient of Thermal Expansion

* Near-peritectic composition

Table 1. Physical properties and cost of potential Pb-free eutectic solders [After 2-4]

1. Tin [2]

The ability of Sn to wet and spread on a wide range of substrates has caused it to become the principal component of most solder alloys used for electronic applications. Tin exists in two different forms, white β-tin and gray α-tin, which have different crystal structures in the solid state. White β-tin has a body centered tetragonal structure and is stable at room temperature, whereas gray α-tin possesses a brittle diamond cubic crystal structure and is thermodynamically stable below 13^oC. Therefore, when tin is exposed to repeated thermal cycling, it may experience a phase transformation from white β-tin to gray α-tin, leading to brittle fracture. The addition of alloying elements has been successful in suppressing this phase transformation.

2. Sn-9Zn [2,3]

The Sn-9wt%Zn alloy is an attractive alternative with a eutectic melting temperature of 198^{o}C, which is relatively close to eutectic tin-lead. The solidified microstructure exhibits large grains with a fine uniform two-phase eutectic colony. Compared to the Pb-Zn system, in the Sn-Zn system, both Sn and Zn react with Cu to form intermetallic phases.

3. Sn-0.7Cu [2,3]

The Sn-Cu binary system has a eutectic composition of Sn-0.7 wt.% Cu and a eutectic temperature of 227^{o}C. The solidification reaction consists of Cu precipitated in the form of hollow rods of the intermetallic Cu_6Sn_5 in tin matrix. Due to the high concentration of tin in this alloy, it may be prone to whisker growth or transform to gray α-tin.

4. Sn-58Bi [2,3]

The Sn-Bi alloy has a eutectic composition of 42Sn-58Bi and a relatively low eutectic melting point of 139^{o}C. At moderate cooling rates, the eutectic Sn-Bi microstructure is lamellar, with degenerated material at the boundaries of the eutectic grains. Recrystallization of the alloy produces large expansion that results in embrittlement of the alloy.

5. Sn-3.5Ag [2,3]

Eutectic Sn-Ag solder has received much attention as a potential Pb-free candidate for electronic and automotive applications. The eutectic solder is non-toxic, has a high eutectic melting point of 221^{o}C, and generally exhibits better mechanical properties than the eutectic Sn-Pb solder. This solder also shows comparable wetting characteristics to eutectic Sn-Pb solder. The microstructure consists of Sn and Ag_3Sn in the form of thin platelets. McCormack *et al*. [2] described the solidified microstructure of the binary eutectic Sn-3.5% Ag consisting of a primary β-Sn phase with dendritic globules and inter-dendritic regions with a eutectic dispersion of Ag_3Sn precipitates with

in a tin matrix. Addition of 1% Zn has been shown to improve the solidification microstructure by eliminating the β-Sn dendritic globules and introducing a finer and more uniform two-phase distribution throughout the alloy. The addition of Zn suppresses the formation of β-Sn dendrites and results in a uniform dispersion Ag_3Sn.

C. NEED FOR A CREEP TESTING TECHNIQUE

A Pb-free solder candidate should have a stable microstructure, exhibiting good thermal fatigue and creep resistance. There are also other factors that should be considered such as melting temperature, solderability, thermal expansion coefficient, interfacial intermetallic compound (IMC) layer growth, cost, etc, for a Pb-free solder candidate to be acceptable in the industrial applications. The shortcomings in the required properties can increase the possibility of solder joint failures during manufacturing and service, causing open circuits and/or mechanical failure of electronic modules [1].

The Pb-free candidate must be tested for various requirements discussed above to determine whether they are suitable as a Pb-free solder replacement. Since the solder joint operates in a cyclic manner in actual service condition, it undergoes thermally induced cyclic fatigue. Also, due to the low melting temperature of solder materials, creep deformation becomes significant even in an ambient environment. In order to predict the reliability of solder joint, the mechanical properties of a solder joint should be assessed. An appropriate model can then be developed to access reliability of the solder joint based on lifetime estimation in the development of a superior Pb-free alternate. Since the solders are susceptible to changes in microstructural evolutions, the microstructural changes should be taken into account in the analysis of solder joint reliability.

The primary method for testing the creep behavior of an electronic solder joint has been based on a lap shear specimen, wherein an array of solder joints between two substrates is tested in shear [e.g.,14-17]. In this method a single solder ball joint or an array of solder balls is made between two substrates. The two substrate components are then pulled in opposite directions creating a shear on the solder balls. The sample

preparation requirements for this type of test are time-consuming and costly. This is because an array of solder balls must be made on one of the substrate components and then the solder must be reflowed a second time to connect the second substrate component. Special car must be used to ensure the solder is reflowed correctly and all connections are made properly. This set up is only good for one test and a new joint must be made for each additional piece of data. This limits the volume of data that can reasonably be generated when compared to the approach employed in this study.

Although nominally loaded in shear, the actual joint stress state in a lap-shear specimen may be quite complicated, particularly when the joints are produced between unlike materials (e.g., between a Si-chip and a plastic substrate, making the results unreliable. The round solder ball will have high stress concentrations at the corners where the solder ball meets the substrate and varying stress through the solder ball. Additionally, this specimen geometry is particularly prone to early damage initiation in one or more joints. This early damage will severely shorten and possibly distort the steady state creep region. Another result of this early damage is a prolonged tertiary stage. Also, since it is very difficult to ensure that each joint in the tested array is defect-free and microstructurally identical to every other joint, the test results are at best an average joint behavior. In a recent review of creeping solder joints, Igoshev and Kleiman [17] supported these reasons. They stated the apparent steady state creep rate may include a component due to internal damage initiation (e.g.,via intercrystalline void nucleation and growth), thereby confounding the creep data [17]. In light of this flaw in conventional creep testing, in order to determine the true creep behavior of solder alloys, these internal damage mechanisms must be suppressed. Therefore there is a need for a more reliable approach that requires minimal sample preparation, is easy to implement and analyze, has high throughput, and is able to probe each solder joint individually.

D. CREEP

Creep is time dependent deformation of a material when it is subjected to a constant load at a constant temperature and is important at temperatures greater than $0.3T_m$. Creep strain is measured as a function of time and the slope of the creep strain vs.

time curve is referred to as the steady state creep strain rate. The creep curve is commonly defined by reference to three different stages as shown in Figure 2, i.e. primary, secondary and tertiary stages [6]. With a constant load applied to a specimen, the strain rate decreases during the primary stage after an instantaneous strain on loading, indicating the material experiences an increase in creep resistance or strain hardening. After the primary stage, strain-rate reaches a secondary stage where the strain rate is constant. The constant strain rate in the secondary stage is explained on the basis of a balance between the competing processes of strain hardening and recovery. The secondary stage often has the longest duration in the lifetime of a material during creep deformation. During the tertiary stage, the strain-rate rapidly increases with time leading to fracture. An increase in strain-rate in the tertiary stage is related to microstructural changes such as grain boundary separation, the formation of cracks, cavities, voids and neck formation, resulting in a decrease in the effective load carrying area.

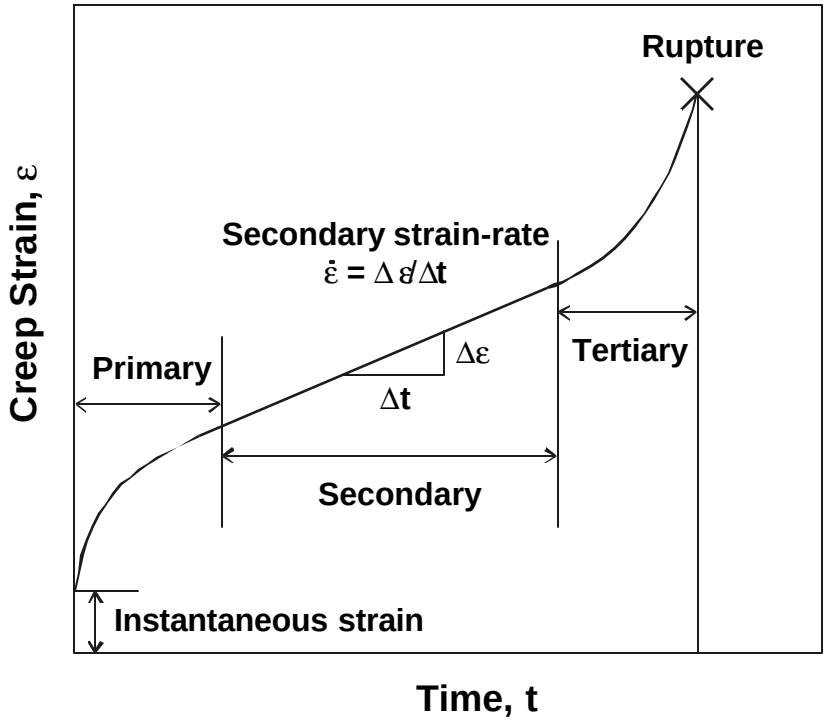

Figure 2. Schematic representation of a creep curve illustrating different creep deformation stages [From 6].

E. IMPRESSION CREEP

1. Introduction

A technique for impression creep testing was first reported in 1977 on a molecular crystal that crept at room temperature [10]. The use of impression testing to characterize the creep properties of materials has shown that both the stress and temperature dependencies of the steady state impression velocity agree with the corresponding dependencies of the creep rate in conventional creep tests [6]. Hence the impression creep test has been established as a convenient way of obtaining extensive creep properties from a limited supply of materials.

The technique for impression creep testing uses a constant diameter cylindrical indenter to impress a constant load onto the surface of a flat sample. Impression creep approach allows steady state to be established a relatively short period of time. Load/indenter area is the punching stress σ, which is constant for constant load and indenter area. Under this stress, the indenter sinks into the material to a depth h in time t. The measure of dh/dt is referred to the creep rate [4]. The steady state impression velocity is a power function of punching stress and for the same punching stress; a plot of log impression velocity versus the reciprocal of absolute temperature yields activation energy [10]. Figure 3 shows how the cylindrical indenter penetrates the surface of a sample over a period of time.

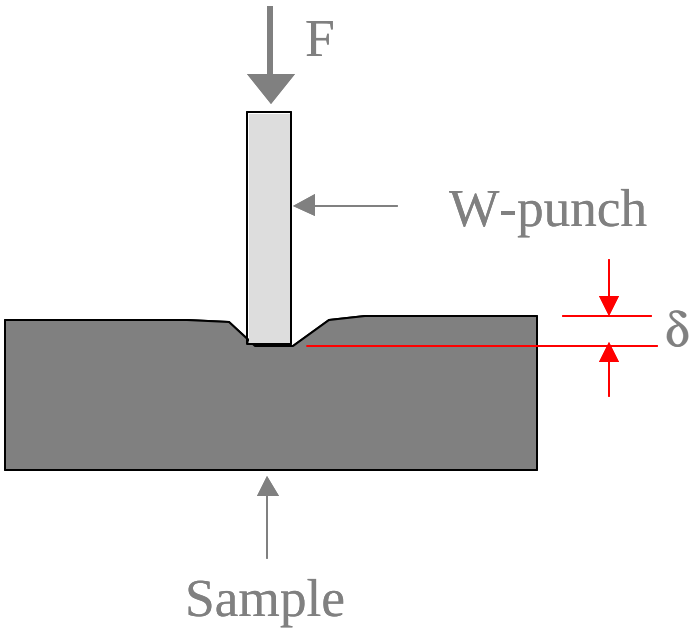

Figure 3. Impression creep of a flat cylindrical indenter on a flat sample

Three mechanisms are possible during impression creep. They are: (1) the dislocation motion in the specimen, (2) interface diffusion between the punch and the specimen, and (3) bulk diffusion inside the specimen [6]. Since all three mechanisms can operate simultaneously in parallel, the overall impressing velocity is the sum of each mechanism.

The mechanism of dislocation creep is by the generation and motion of dislocations. The impression velocity, $v_{d,}$ is calculated numerically by finite element method. A power law constitutive equation is assumed to be valid for each finite element at steady state [6]. This power law is between the creep rate and the Von Mises stress. The Von Mises flow rule is used to calculate the various strain components. The calculation is done over many time intervals until a trend toward steady state is clearly indicated [6]. The result is that the Von Mises stress available for creep at any distance relative to the punch radius is found to be proportional to the applied punching stress. As a result the steady state impressing velocity is proportional to the punch radius, and has the same stress dependence as the steady state creep rate. The calculated impression

velocity agrees well with the experimental value for the same conditions. For the power law equation,

$$\dot{e}_e = As_e^n \tag{2}$$

where $\dot{e}$ is the unidirectional creep rate, σ_e is the unidirectional stress, and A and n are constants at constant temperature. The impressing velocity may be expressed by:

$$v_d = 2Aa(s/m)_e^n \tag{3}$$

In bulk diffusion the path of vacancy diffusion starts from the free surface, passes through the bulk and terminates under the indenter. The vacancy arrival under the indenter should be at a rate consistent with the impressing velocity v_b [6]. For a mean stress a mean relation is found between the impressing velocity and the impressing stress σ;

$$v_b = \frac{3pVD}{4aRT} \tag{4}$$

where $D=D_v c_v V$ is the self diffusivity of atoms, D_v is the diffusivity of vacancies, c_v concentration of vacancies, R is the gas constant, T is the absolute temperature, and V is the molar or atomic volume of atoms [6]. This equation shows that for the same impression stress, the impression velocity is inversely proportional to the radius of the punch.

In addition to the bulk diffusion mechanism, the indenter can descend due to the surface diffusion of atoms or molecules along the interface between the indenter and the crystal. A relation between the impressing velocity v_s due to surface diffusion and the indenter stress σ can be shown by;

$$v_s = \frac{8D_s c_s V^2 s}{a^2 RT} \tag{5}$$

where D_s is the self diffusivity, and c_s is surface concentration of atoms outside the indenter [6]. This equation shows that for the same punching stress, the impressing velocity is inversely proportional to the area of the indenter. In addition to the stress and

indenter size dependencies of impressing velocity, the temperature dependency should reveal the activation energy for surface diffusion, which should be smaller than bulk diffusion.

Li et. Al. [6] made a direct correlation between indenter size and creep mechanisms. He determined that for small indenter sizes (.1-.6mm) surface diffusion would be the dominant mechanism. For intermediate sized indenters (.6-8mm) bulk diffusion would become dominate and as indenter size further increased dislocation creep would eventually dominate. Since there is no clear start and stop point for any one mechanism there are regions over which two or all three mechanisms may operate simultaneously.

2. Experimental Observations on Different Materials

Metals and alloys are the materials most studied by conventional creep and hence, they have been studied most by impression creep. Chu and Li [11] conducted impression creep experiments on β-tin single crystals in three orientations, [001], [100], and [110]. The temperature dependence of impression velocity showed two parallel processes. The first was the activation energy for the high temperature process. This was found to be the same for all three orientations, independent of stress and comparable to that for self-diffusion. The second was the activation energy for the low temperature process. This was found to be orientation dependent. Calculated power law values and activation energy compared closely with conventional creep test results. The high temperature process was credited to dislocation climb while the low temperature process was determined to be dislocation slip [6].

Godavarty and Murty [12] applied impression creep to a polycrystalline zinc sample and showed differences on three different faces due to grain size and/or texture effect. However, the activation energy was the same for all three orientations. Similar to Li's experiments on β-tin activation energy depended on temperature.

Hyde et al.[18] conducted impression creep tests on a 316 stainless steel at 600^{o}C on the same specimen over which a conventional uniaxial creep test was performed. The tensile specimen was cut in the middle and a zirconia cylinder of 1.5 mm diameter was inserted between the two halves. It was shown that when the impression creep data was

converted to uniaxial data based on the reference stress approach, the two sets of data agreed very well with each other [10]. It was noted that since the effective gage length was very small in the case of impression creep, the displacement measurement must be conducted very accurately when compared with uniaxial testing for which gage length is considerably larger [10]. Similarly, the load measurement must be conducted more accurately too for impression creep due to the small cross-sectional area.

Juhsz et al. [12] performed impression creep on Pb-Sn eutectic alloys using a stainless steel cylindrical indenter of 1mm diameter. At lower strain rates, the stress showed superplastic behavior. The activation enthalpy was found stress dependent. The results obtained were in good agreement with conventional tensile tests using many specimens.

Glass ceramics and ionic crystals are all subject to creep at high temperatures. Yu and Li [6] studied impression creep of single crystal LiF. Both the stress exponent and activation energy were comparable with those obtained by conventional creep of the same crystal under similar conditions.

3. Applications of Impression Creep Testing

Weldments are a proper place for performing impression creep because it is difficult to make uniform tensile specimens from the jointed areas. Yu et al. [13] studied the mechanical properties of high energy laser beam welds in A36 steel by using impression tests at constant punch penetration rates. The yield strength, ultimate tensile strength, strain rate sensitivity, strain hardening coefficient, ect. Obtained at the fusion zone, heat affected zone and the base metal in the as welded condition and after stress relief were reported.

Application of impression creep in FC and BGA systems will allow rapid testing of individual solder balls of FC and BGA components. This is because tests will be accomplished on individual solder balls. Therefore numerous data points can be generated from one sample. As stated previously, this is opposed to convention creep testing where only one data point could be generated from one sample.

From this discussion it is clear that impression creep can be used in place of conventional creep testing, which is time consuming and inconvenient. In some cases,

impression creep technique is the only process possible such as in weldments or during irradiation [6]. Some other advantages of impression creep testing are as follows: small amount of testing material, stress and temperature effects tested on the same crystal, stable deformation without tertiary stage, constant stress at constant load, separation of creep mechanisms by punch size in addition to stress and temperature effects, and possible direct determination of self diffusivity [5].

III. EXPERIMENTAL SETUP

A. APPROACH

1. Experimental Set Up

The MTS Corporation's 810 Material Test System (MTS) was the base platform used for setting up a vertical impression creep experiment. Figure 4 shows a schematic of the impression creep apparatus. The following equipment was used for data acquisition and experiment control:

1. The Teststar II data acquisition and control system was used to control the MTS hydraulic system and collect data from each measurement device. The analog to digital converter within the Teststar II digitized the signals from the load cell, temperature controller, and capacitance gauge to load, temperature, and impression depth, respectively. The digitized signals were sent to a personal computer for recording and data processing.
2. A Sensotech 50 lb load cell was used for force measurements and constant force control. Maximum force fluctuation during any given test was ± 0.1N.
3. A Capacitec series 4000 high temperature capacitance gauge continuously monitored impression depth. The capacitance gauge was calibrated over a range of 0-250μm. Maximum fluctuation in displacement measurement during any given test was ± 0.1μm.
4. An Omega I-series temperature controller was used for temperature control. Maximum temperature fluctuations for any given test was ± 0.5^{o}C.
5. An impression platform was designed and constructed to hold a sample, heaters, thermocouple and the capacitance gauge in a compact structure. All load-bearing components were constructed of stainless steel. The platform was insulated with low thermal conductivity (k=.41W/m^{o}K) machinable ceramic, purchased from AREMCO Inc, to minimize heat loss through the platform. To maintain a constant temperature atmosphere around the sample and minimize heat effects on external components a ceramic enclosure was constructed around the platform.

6. A 1mm diameter tungsten carbide rod was used as the indenter. The rod was cut flat and polished. The indenter was inserted into the stainless steel indenter assembly.
7. The hydraulic ram of the MTS 810 hydraulic system was used to apply and maintain constant force on a specimen. A program written using Teststar II software collected data and controlled the MTS ram movement.

MTS 810 tuning parameters are as follows:

Hydraulic Parameters

Valve Balance 1	-0.4405
Valve Balance 2	0.0002
Dither Amplitude	0.0050V
Dither Frequency	550.00 Hz

Force Parameters

P Gain	90.00	scale 0-200
I Gain	70	scale 0-100
D-Gain	0	
F Gain	0	
Fl Filter	2048	

Displacement Parameters

P Gain	60.9323	scale 0-100
I Gain	.1018	scale 0-1
D Gain	0	
F Gain	0	
Fl Filter	2048	

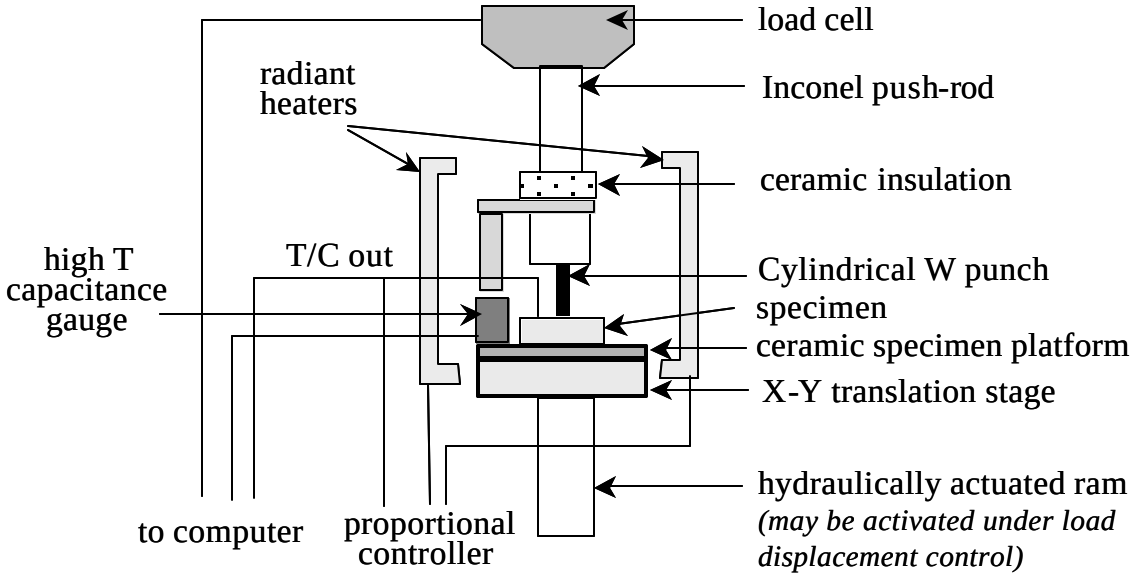

Figure 4. Schematic of experimental apparatus for Impression Creep.

2. Sample Preparation

Fine microstructures are normally seen in freshly re-flowed solder balls used in microelectronics. This microstructure coarsens over time due to strain enhanced aging during thermal cycling. For this reason two sets of samples were made. The first set consisted of a fine microstructure while the second set underwent an aging process to coarsen its microstructure.

A 3 lb. bar ingot of eutectic Sn-Ag alloy was provided from Alpha Metals Inc. The as-received ingot consisted of a very coarse microstructure, which was not common to that seen in microelectronics. Twelve 5.5 gram specimens were cut from the eutectic bar and re-flowed. The specimens were heated in a small cylindrical aluminum crucible on a hot plate until the sample was completely melted. The sample was then placed in a furnace until the molten solder stabilized at a temperature of 225^{o}C. The crucible was then placed on an aluminum plate, maintained at room temperature, for 15 seconds. The specimen was subsequently quenched in a water bath. This procedure produced a fine

microstructure, which will be further explained in the next section. The samples were then polished to form a small cylinder with flat ends. Six of the twelve re-flowed specimens were heat treated at 180^{o}C for 100 hours in order to coarsen the fine microstructure of the as reflowed specimen.

IV. MICROSTRUCTURE ISSUES

The typical microstructure of the eutectic Sn-3.5Ag alloy produced in microelectronic solder joints, consists of a fine Ag_3Sn intermetallic phase dispersed in a uniform β-Sn matrix. For bulk samples, however, the solidification of the eutectic Sn-Ag alloy produces a microstructure of off-eutectic composition that consists of a primary β-Sn phase and a eutectic Sn-Ag phase. This is due to the depression of the eutectic temperature and an associated shift of the eutectic composition, causing the alloy of eutectic composition (Sn-3.5Ag) to produce an off-eutectic microstructure. Figure 5 illustrates the depression of the eutectic temperature and under-cooling required to nucleate eutectic composition. The depression of the eutectic appears to occur because the first nucleated phase (Sn) is a poor nucleant for the second phase (Ag_3Sn) [4]. A substantial under cooling below the true eutectic temperature is required before the eutectic phase is nucleated. As a result, primary Sn phase solidifies first and then eutectic Sn-Ag microstructure is formed as shown in Figures 6. Most published micrographs of eutectic Sn-3.5Ag solder show the presence of primary Sn phases [4].

The relationship of under cooling and cooling rate is a complex issue. A fast cooling rate will most likely result in a high under cooling. However, an extremely slow cooling rate can also result in a high under cooling if no heterogeneous nucleation sources exist. This is shown in Figure 7 as areas of primary Sn can be seen in a slow cooled sample of eutectic Sn-Ag. As cooling rate is further decreased Ag_3Sn phase forms needles and coarsen into plates as cooling rate is even further decreased.

A pure eutectic microstructure was desired for this study. However, producing the eutectic structure in a bulk sample proved to be very difficult. Numerous processes and cooling rates where tried in an attempt to generate the eutectic microstructure. Figures 7-9 show some of the processes and resulting microstructures.

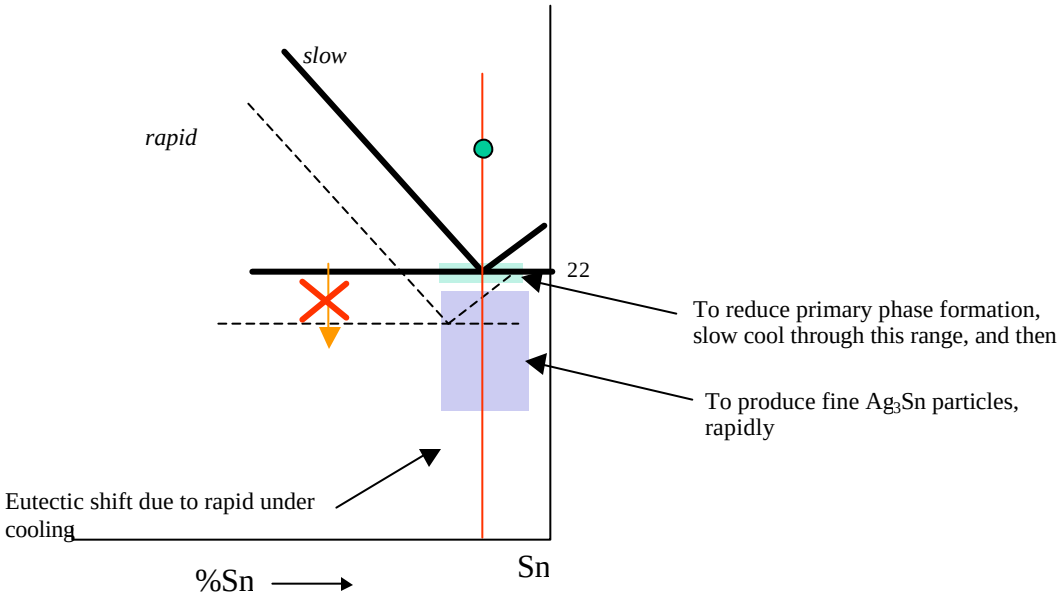

Figure 5. Eutectic shift in Sn-3.5 Ag Schematic of the Sn end of the Sn-Ag phase diagram, illustrating the shift in eutectic temperature and composition due to non-equilibrium cooling.

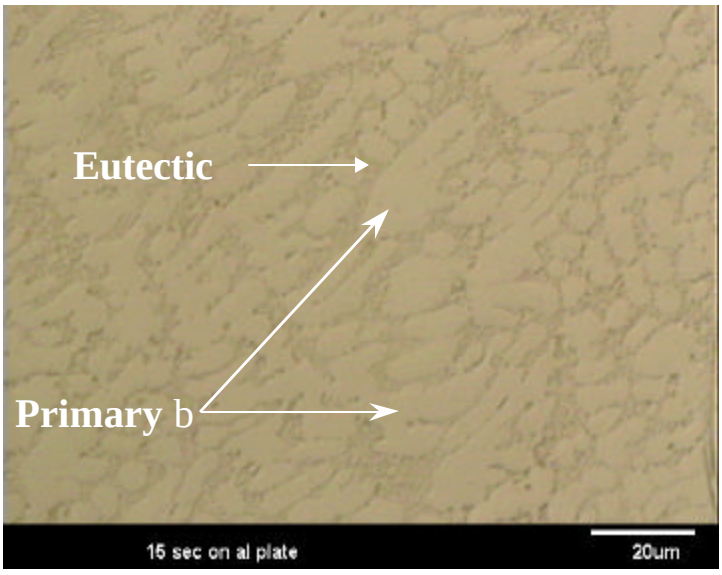

Figure 6. Microstructure of fast cooled Sn-3.5Ag, showing primary phase dendrites, with the eutectic microstructure in the intermediate spaces. This sample was heated to 256C then immediately quenched in ice water.

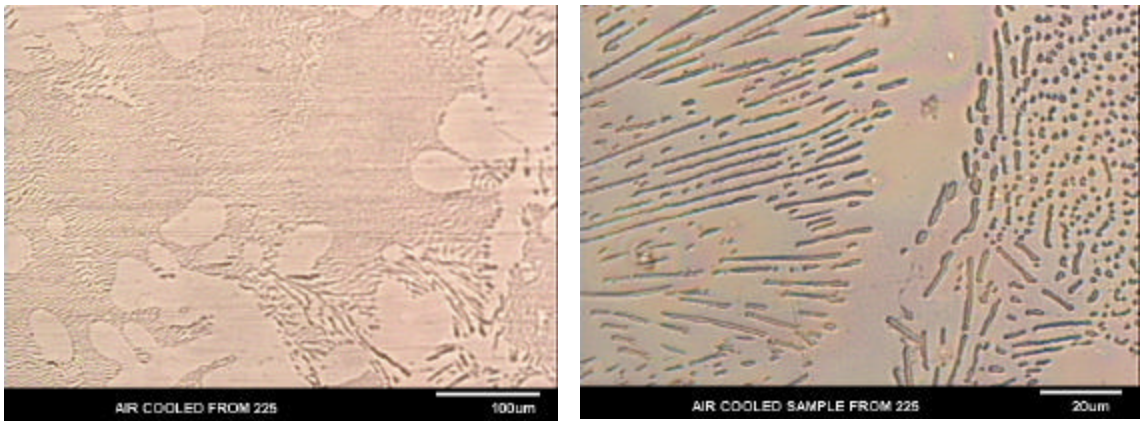

Figure 7. Microstructure of slow cooled Sn-3.5Ag, showing primary phase dendrites, with a coarse eutectic microstructure and needles in the intermediate spaces. This sample was heated to 225C in a graphite crucible on a hot plate, slow cooled to 217C, then quenched in water.

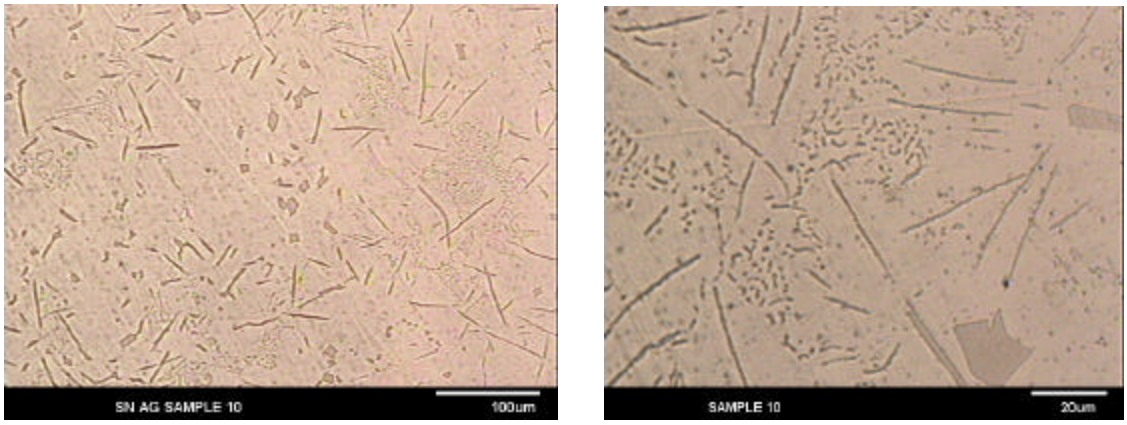

Figure 8. Microstructure of slow cooled sample, showing a combination of coarse particles, needles, and platelets. This sample was liquefied at 225^{o}C in a furnace, slow cooled in furnace to 221.3^{o}C, removed from furnace and air cooled to 217^{o}C, and then quenched in water.

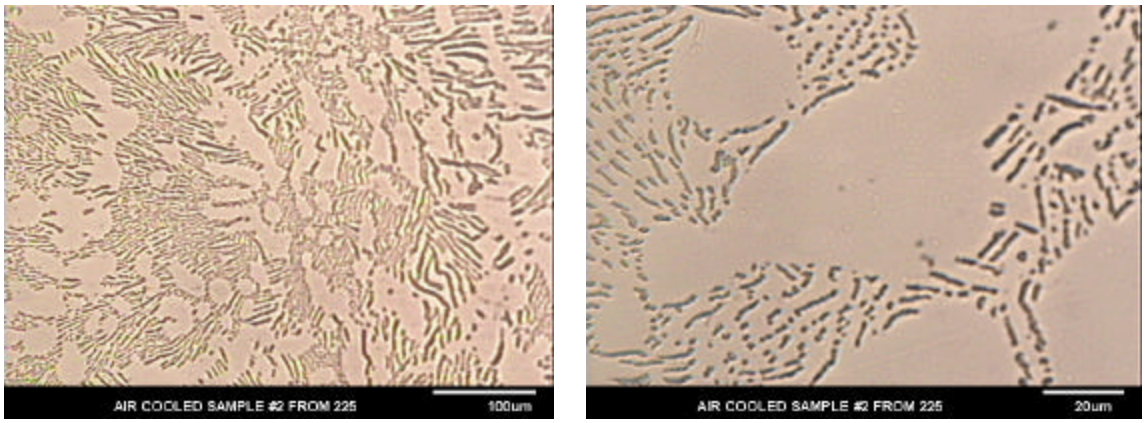

Figure 9. Microstructure of moderately cooled Sn-3.5Ag, showing primary phase dendrites surrounded by Ag_3Sn needles. This sample was liquefied at 225°C in a furnace, slow cooled in furnace to 221.3°C, removed from furnace and fan cooled to 217°C, and then quenched in water.

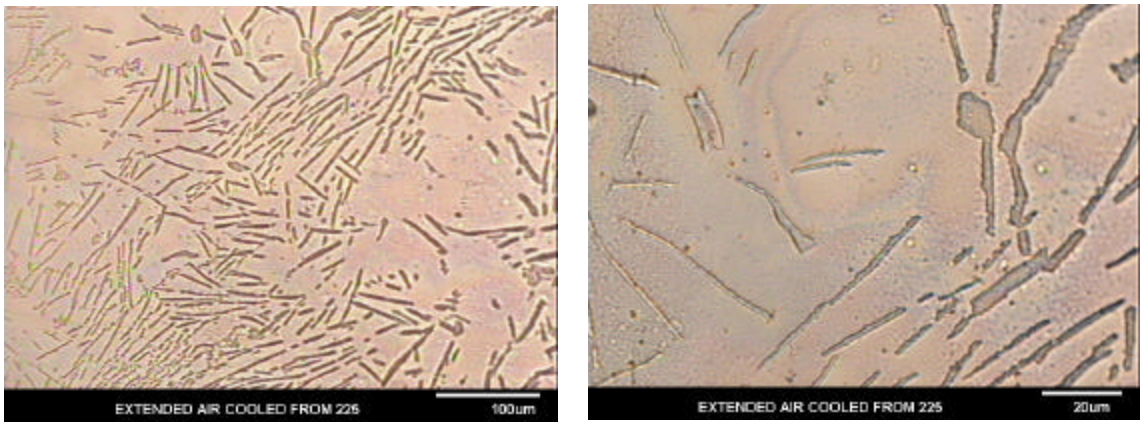

Figure 10. Microstructure of slow cooled sample showing a combination of needles and platelets. This sample was liquefied at 225°C in a furnace, slow cooled in furnace to 221.3°C, removed from furnace and air cooled until solidification was complete, and then quenched in water.

V. SAMPLE MICROSTRUCTURE

Since the eutectic microstructure could not be produced in samples large enough for testing on the constructed apparatus a microstructure consisting of Sn dendrites and very fine Ag_3Sn particles was chosen. This microstructure was chosen for two reasons. The first reason is that this microstructure has been seen in some electronic applications. The second reason is that it contains a phase of fine Ag_3Sn particles in the intermediate regions of primary β-Sn, which can be aged and coarsened. SEM photographs of an unaged test sample are shown in Figures 11 and 12. The fine Ag_3Sn particles can be seen surrounding primary tin regions. The second set of samples was coarsened by heat treating the samples at 180C for 100 hours. The coarsened microstructure was then tested to see the effects of coarsening on creep behavior. Figures 13 and 14 show SEM photographs of a sample after aging.

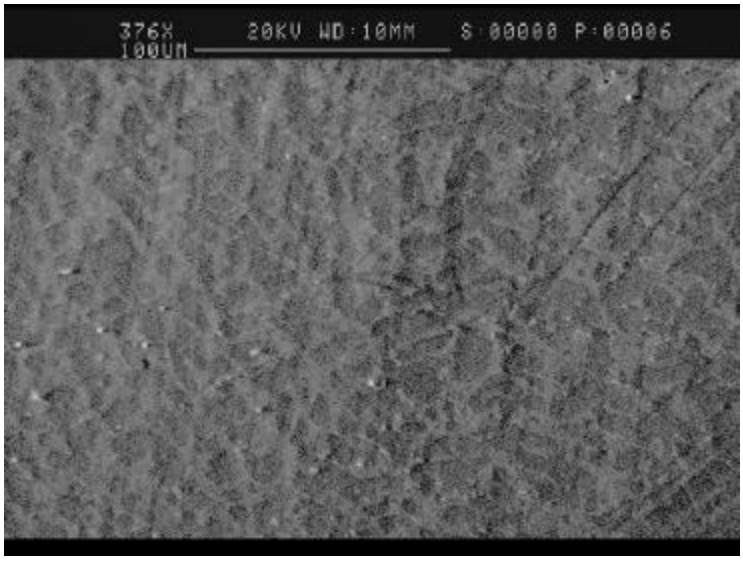

Figure 11. SEM photograph of an unaged sample.showing fine Ag_3Sn particles in intermediate spaces.

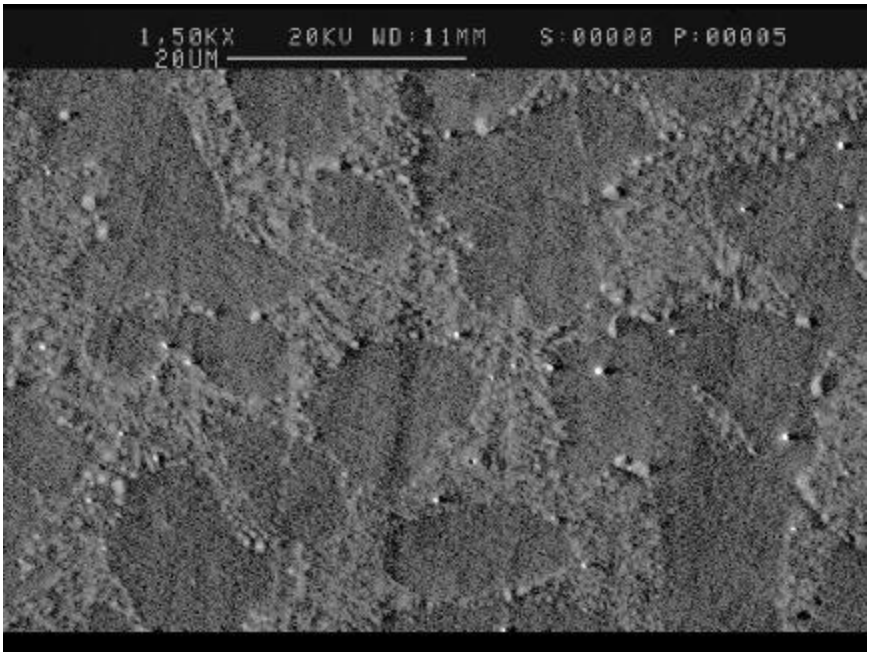

Figure 12. SEM photograph of unaged sample showing fine Ag_3Sn particles in intermediate spaces.

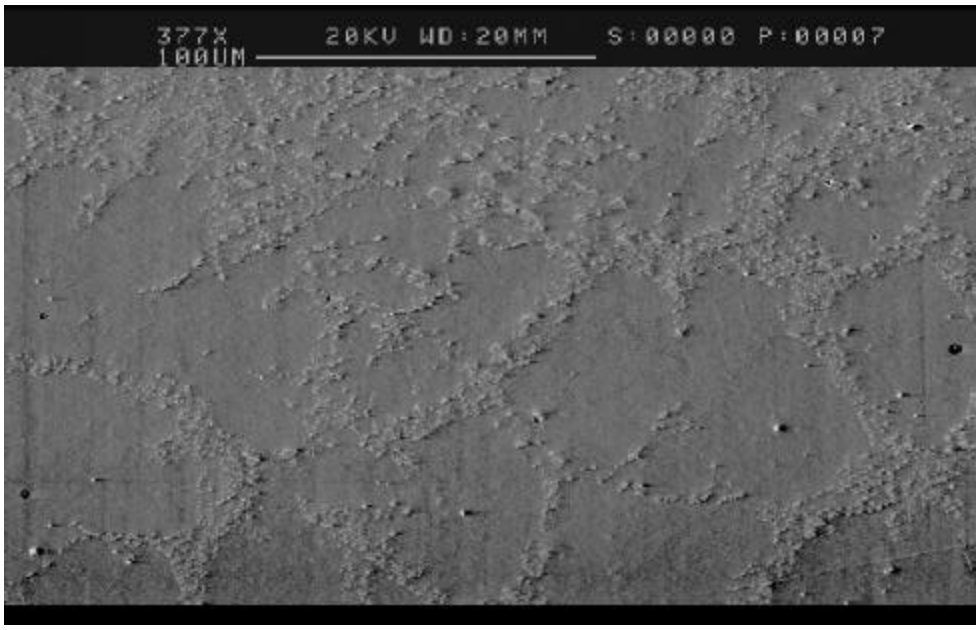

Figure 13. SEM photograph of aged test sample showing primary phase and coarse Ag_3Sn particles in intermediate spaces

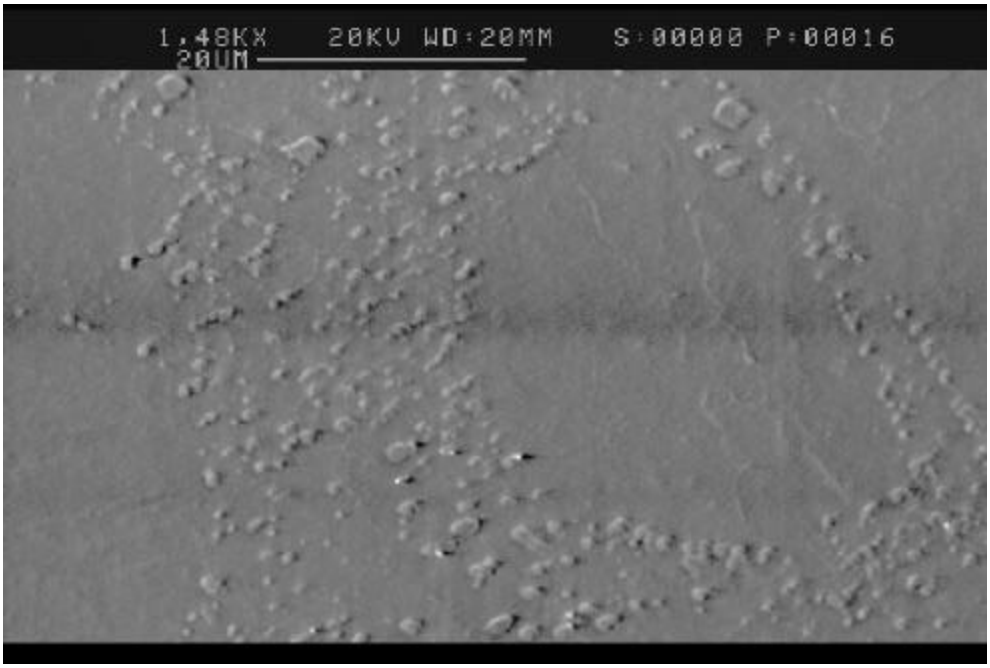

Figure 14. SEM photo of test sample after being aged 100 hours at 180C showing coarsened Ag_3Sn particles.

THIS PAGE INTENTIONALLY LEFT BLANK

VI. TESTING RESULTS

To show that the impression velocity reaches a steady state, a typical impressing depth time curve is shown in Figure 15 for several punching stresses. It is clear in this figure that after a brief period each plot reaches a constant slope. These plots are of raw unmodified data. The slight distortion in each plot is due to minor temperature fluctuations during testing. Plotting the steady state velocities from this figure as a function of stress using a log-log scale will result in a straight line. The slope of this line gives the stress exponent n for the power law equation (equation 1) [14].

Figure 16 shows impression depth time curves for a constant stress at different temperatures. This plot shows the effects of temperature on creep rate as impressing velocity increases with increasing temperature. It can also be seen in this case, as in the previous tests, that a steady state for the impressing velocity is reached after an initial transient period. Plotting these steady state velocities vs. 1/T (Temperature in K) will yield the activation energies. Figure 17 shows a plot of the values from Figure 1 vs. 1/T. This preliminary data used to generate this plot agrees closely with published data for eutectic Ag_3Sn. Further test must be completed to before actual determination of activation energy can be made.

It was expected that microstructural coarsening would affect creep characteristics of the Sn-Ag samples. Figure 18 confirms this expectation. Figure 18 shows a comparison between the steady state impression velocities of an aged and unaged sample at the same stress and temperature. It is clear in this figure that the aged sample impresses at a much higher rate than the unaged sample. This is important as it shows that microstructural change must be considered when modeling creep characteristics of eutectic Sn-Ag.

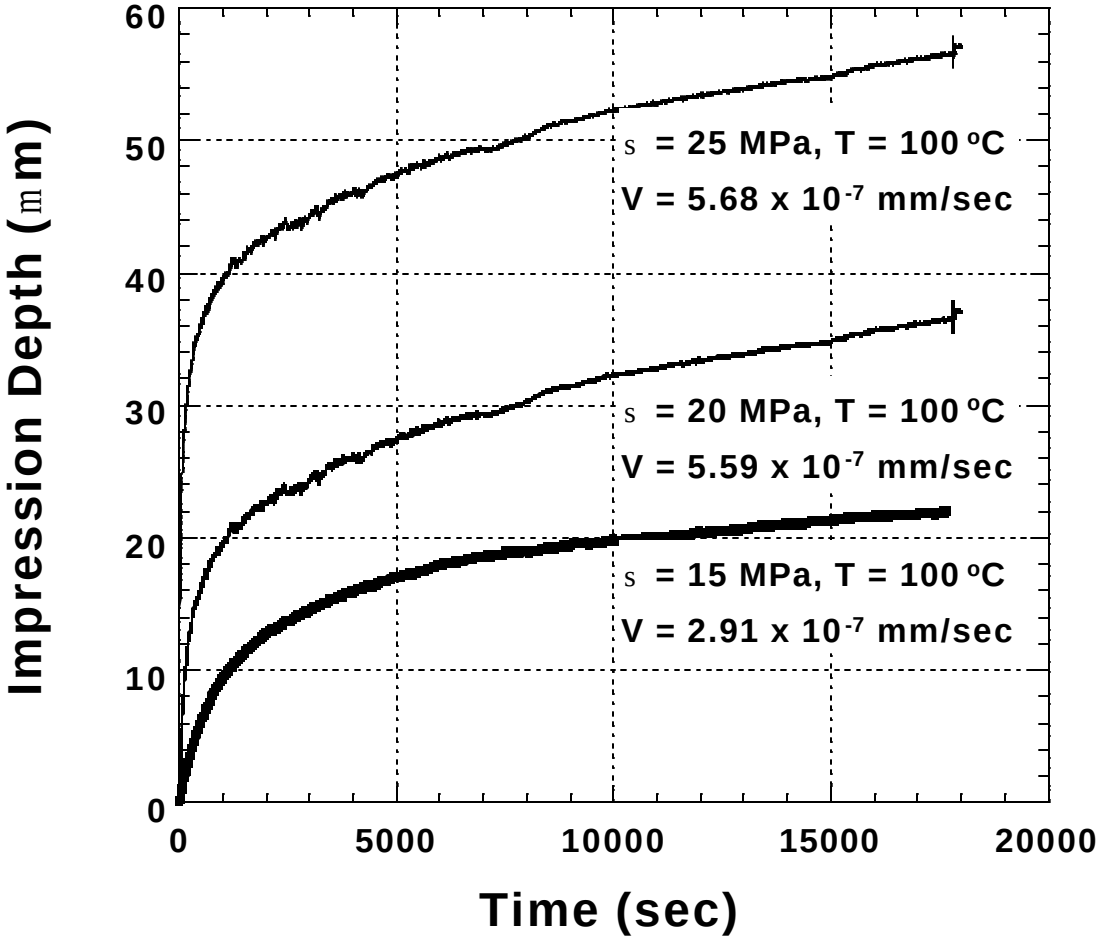

Figure 15. Impression creep curves of the aged Sn-Ag eutectic alloy for different stresses at 100°C

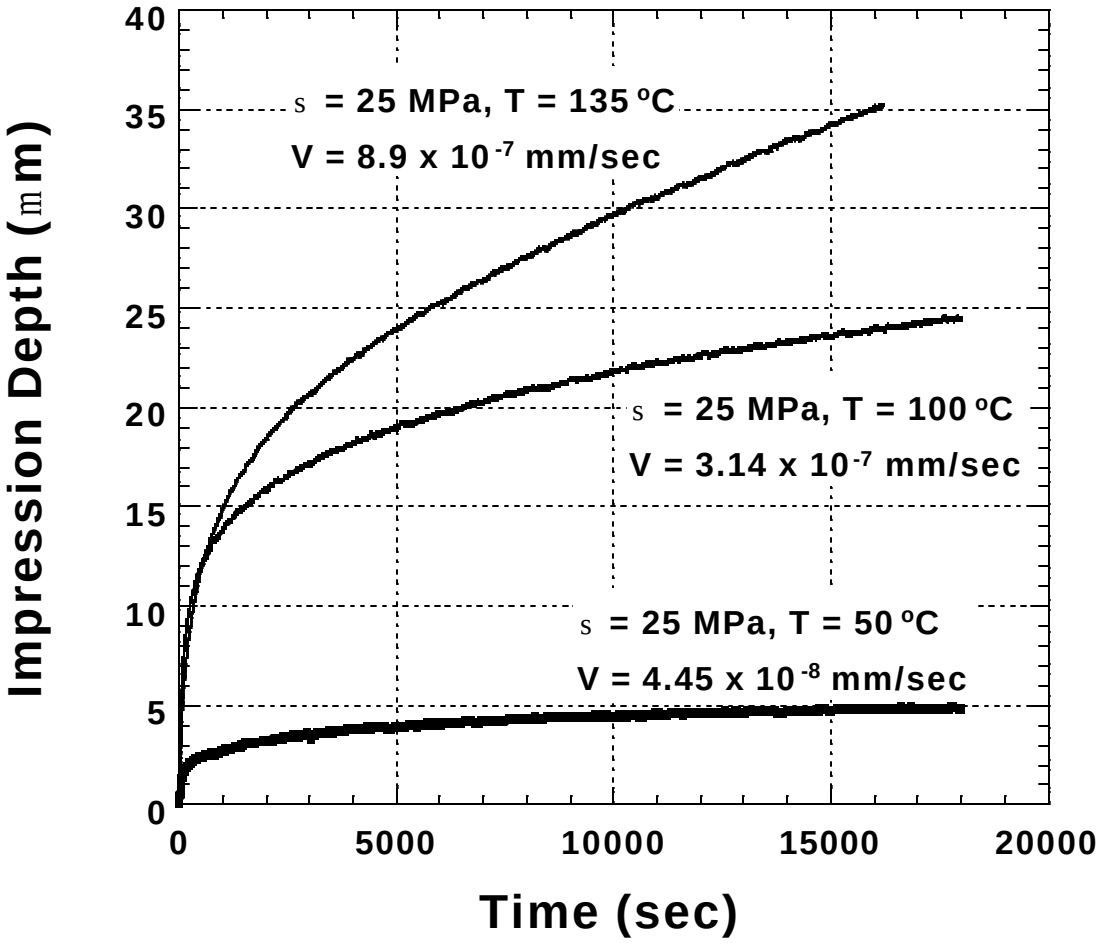

Figure 16. Impression creep curves of the unaged Sn-Ag eutectic alloy for different temperatures at a stress of 25 MPa.

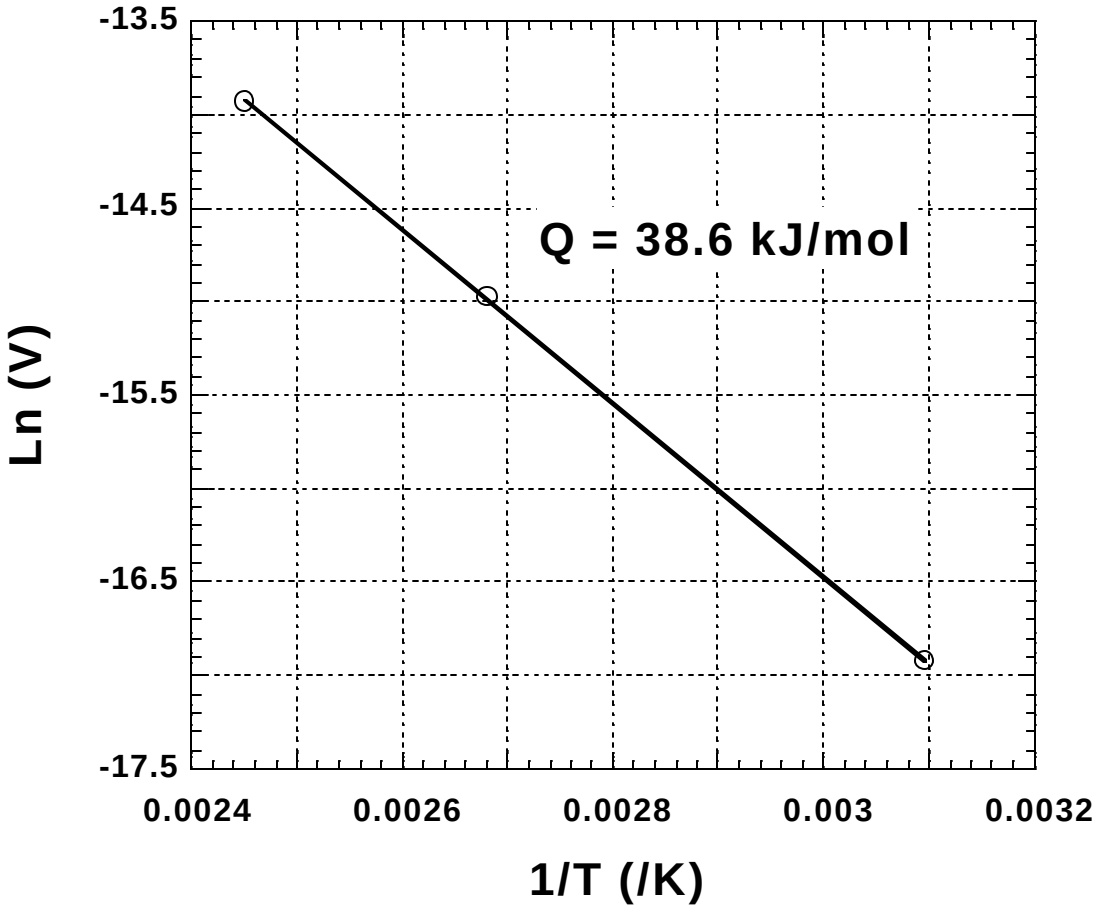

Figure 17. Activation energy for impression creep of unaged Ag_3Sn test sample.

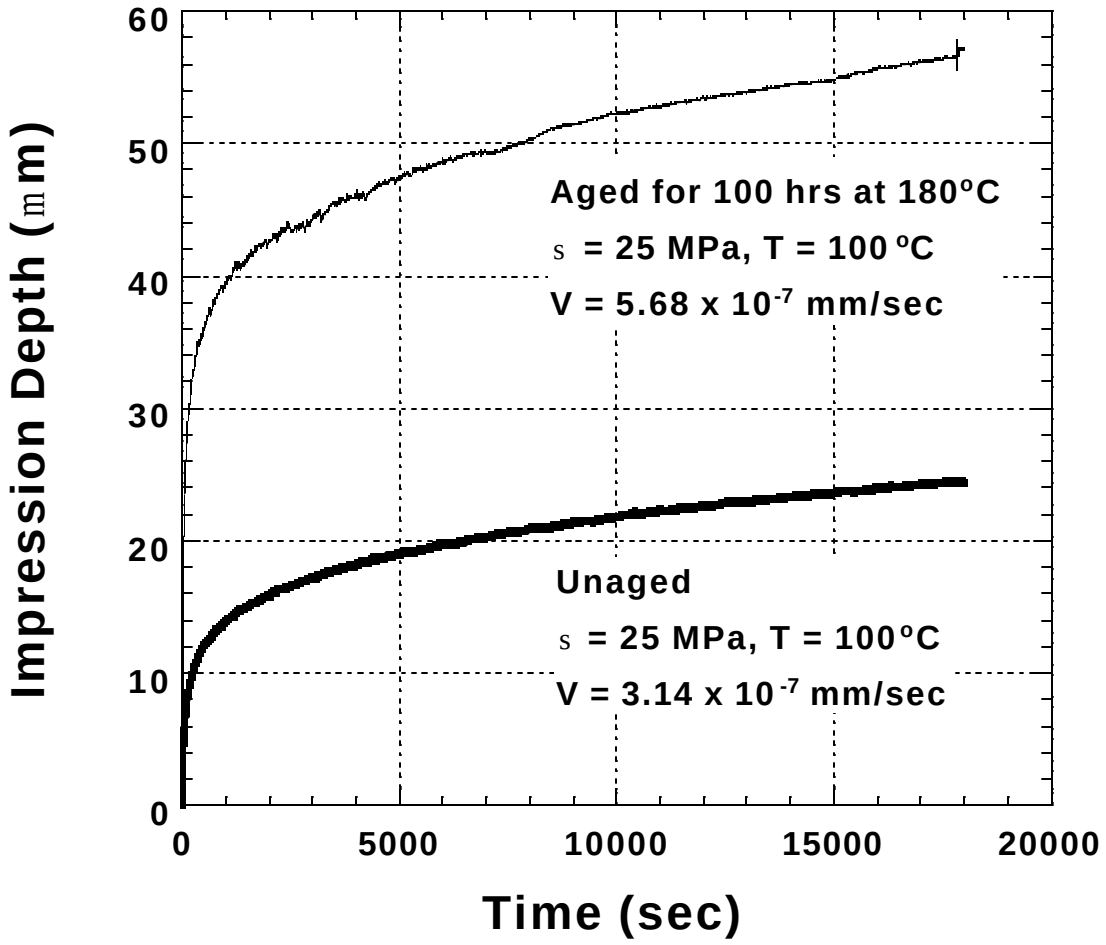

Figure 18. Impression creep curves of an unaged test sample and an aged sample showing the aged sample having a higher impression steady state velocity.

THIS PAGE INTENTIONALLY LEFT BLANK

VII. CONCLUSION

Various reflow conditions were investigated to produce desired microstructures in Sn-3.5Ag lead free solder. Two microstructures, one as reflowed and one aged at 180C for 100 hours, were selected for testing in order to discern the impact of microstructural coarsening in the creep behavior of Pb-free alloys.

A creep apparatus was constructed using a servo mechanical test frame, with a ±0.1N load stability and ±0.1μm displacement stability. These performance parameters where achieved using the tuning specifications outlined in this Thesis. Preliminary creep data were generated on the aged and unaged solder microstructures. The high resolution of the apparatus resulted in precise impression creep curves, and showed that the aged microstructure creeps more rapidly than the unaged microstructure. In the future this apparatus will be used for testing tiny lead free solder balls used in microelectronics.

THIS PAGE INTENTIONALLY LEFT BLANK

LIST OF REFERENCES

1. The International Technology Roadmap for Semiconductors, Semiconductor Industry Association, San Jose, Ca,1999

2. McCormak M., Jin, s., and Kammlott, G.W. "New Pb-free Solder Alloys with Improved Properties", *IEEE*, pp.7803-2137-5/95, 1995

3. Hua, Fay and Glazier, Judith, "Lead-Free Solders for electronic Assembly", Electronic Assembly Development Center, Hewlett-Packard Company, Palo Alto, Ca, 1997.

4. Mulugeta, A. and G. Selvaduray, "Lead-free Solders in Microelectronics", *Material Science and Engineering,* vol.27, pp. 95-141, 2000.

5. Li, James C., "Impression Creep and Other Localized Tests," *Material Science and Engineering*, A322, pp23-42, May 2002.

6. Li, J.C. and Chu,S.N, "Impression Creep; A New Creep Test", Material Science Program, Department of Mechanical and Aerospace Science, University of Rochester, Rochester, New York, 1977.

7. Yang, F and Li, J.C. "Impression Tests of 63Sn-37Pb Eutectic Alloy", *Material Science and Engineering*, A201, pp. 40-49, April 1995.

8. Burden, M.H. and Hunt, J.D., *Journal of Crystal Growth*, vol. 22, pp. 328-330, 1974.

9. Chu, S.N. and Li J.C, "Impression Creep", *Material Science and Engineering*, A12 pp. 2200-2208, 1977.

10. Chu, S.N. and Li J.C, "Impression Creep of β-Tin Single Crystals", *Material Science and Engineering*, A39, pp. 1-10, 1979.

11. Juhasz, A., Tasnadi, P., and Szasvari, P., "Impression Creep of Eutectic Sn-Pb", *Material Science and Engineering*, A21, pp. 3287-3291, 1986.

12. Yu, H.Y. and Imam, M.A., "Mechanical Properties of High energy Beam Welds", *Material Science and Engineering*, A64, pp. 55-58, 1985.

13. Yang, Fugian and Li, James, "Impression Test of 63Sn-37Pb Eutectic Alloy", *Material Science and Engineering*, A201, pp.40-49, 1995.

14. Darveau,R. and Baneji, K., "Constitutive Ralations for Tin Based Solder Joints", *IEEE Trans. Comp.*, Hyb. Manuf. Technol., 15, pp. 1013-1024, 1992.

15. Yang, H.,Deane, P., Magil, P. and Murty, K.L., "Creep Deformation of 96.5Sn-3.5Ag Solder Joints in a Flip Chip Package", *Proc 1996 Electronic Comp. Tech Conf.* Pp.1136-1142.

16. Reynolds, H.L.,Kang, S.H. and Morris, J.W., "The Creep Behavior of In-AgEutectic Solder Joints",28, pp. 69-75, 1999.

17. Igoshev, V.I. and Kleiman, J.I., "Creep Phenomena in Lead Free Solders", J. Electronic Mat. , 29, pp. 244-250, 2000.

18. Hyde, T.H., Sun, W., and Williams, J.A., "Material high Temp", *Material Science and Engineering*, pp. 117-129, 1999.

INITIAL DISTRIBUTION LIST

1. Defense Technical Information Center.....1

   Ft. Belvoir, VA

2. Dudley Knox Library.....1
   Naval Postgraduate School

   Monterey, CA

3. Naval/Mechanical Engineering Curricular Office, Code 34.....1
   Naval Postgraduate School
   Monterey, CA

4. Department Chairman, Code ME.....1
   Department of Mechanical Engineering
   Naval Postgraduate School
   Monterey, CA

5. Dr. Indranath Dutta.....1
   Department of Mechanical Engineering
   Naval Postgraduate School
   Monterey Ca

6. LCDR Onofrio A Anastasio.....1
   Cherry Hill NJ